Arsenic trioxide targets MTHFD1 and SUMO-dependent nuclear de novo thymidylate biosynthesis

Elena Kamynina[a], Erica R. Lachenauer[a,b], Aislyn C. DiRisio[a], Rebecca P. Liebenthal[a], Martha S. Field[a], and Patrick J. Stover[a,b,c,1]

[a]Division of Nutritional Sciences, Cornell University, Ithaca, NY 14853; [b]Graduate Field of Biology and Biomedical Sciences, Cornell University, Ithaca, NY 14853; and [c]Graduate Field of Biochemistry, Molecular and Cell Biology, Cornell University, Ithaca, NY 14853

Contributed by Patrick J. Stover, February 12, 2017 (sent for review December 1, 2016; reviewed by I. David Goldman and Anne Parle-McDermott)

Arsenic exposure increases risk for cancers and is teratogenic in animal models. Here we demonstrate that small ubiquitin-like modifier (SUMO)- and folate-dependent nuclear de novo thymidylate (dTMP) biosynthesis is a sensitive target of arsenic trioxide (As_2O_3), leading to uracil misincorporation into DNA and genome instability. Methylenetetrahydrofolate dehydrogenase 1 (MTHFD1) and serine hydroxymethyltransferase (SHMT) generate 5,10-methylenetetrahydrofolate for de novo dTMP biosynthesis and translocate to the nucleus during S-phase, where they form a multienzyme complex with thymidylate synthase (TYMS) and dihydrofolate reductase (DHFR), as well as the components of the DNA replication machinery. As_2O_3 exposure increased MTHFD1 SUMOylation in cultured cells and in in vitro SUMOylation reactions, and increased MTHFD1 ubiquitination and MTHFD1 and SHMT1 degradation. As_2O_3 inhibited de novo dTMP biosynthesis in a dose-dependent manner, increased uracil levels in nuclear DNA, and increased genome instability. These results demonstrate that MTHFD1 and SHMT1, which are key enzymes providing one-carbon units for dTMP biosynthesis in the form of 5,10-methylenetetrahydrofolate, are direct targets of As_2O_3-induced proteolytic degradation, providing a mechanism for arsenic in the etiology of cancer and developmental anomalies.

MTHFD1 | arsenic trioxide | one-carbon metabolism | SUMO-1 | genome instability

Perturbations in de novo thymidylate (dTMP) biosynthesis have been implicated in the pathogenesis of folate-responsive neural tube defects (NTDs) (1, 2). Deoxythymidine triphosphate is produced through both nucleotide salvage and de novo synthesis pathways (3). De novo dTMP synthesis is catalyzed by thymidylate synthase (TYMS), which transfers a one-carbon unit from the coenzyme 5,10-methylenetetrahydrofolate (5,10-methyleneTHF) to uridylate, yielding dTMP and dihydrofolate (DHF). DHF reductase (DHFR) reduces DHF to THF. 5,10-methyleneTHF can be regenerated either from serine and THF through the activity of serine hydroxymethyltransferase (SHMT1 or SHMT2α) or from formate, ATP, NADPH, and THF by the activity of methylenetetrahydrofolate dehydrogenase 1 (MTHFD1) (4–6). SHMT1, DHFR, and TYMS are small ubiquitin-like modifier (SUMO)-ylated and translocate to the nucleus at the G1/S boundary (7–16). During S-phase of the cell cycle, the nuclear de novo dTMP synthesis pathway assembles as a lamin-associated multienzyme complex that consists of SHMT, MTHFD1, TYMS, DHFR, and other components of the replication machinery (12, 13).

Mitochondrially derived formate is the primary source of one-carbon units for dTMP synthesis. Formate translocates to the cytosol and nucleus, where it is conjugated to THF by MTHFD1 (14, 17). SHMT is also a source of cytosolic and nuclear one-carbon units, but makes minor catalytic contributions to dTMP synthesis (Fig. 1) (4, 15, 18). However, SHMT1 is critical for nuclear de novo dTMP synthesis by serving as a scaffold for the assembly of the multienzyme complex (12). De novo dTMP synthesis maintains a pool of deoxythymidine triphosphate nucleotides available for DNA replication and repair, and perturbations in this pathway lead to uracil incorporation into DNA, resulting from increased dUTP levels. Decreased rates of de novo dTMP synthesis can be caused by the action of chemotherapeutic drugs (19), through inborn errors of folate transport and metabolism (15, 18, 20, 21), by inhibiting translocation of the dTMP synthesis pathway enzymes into the nucleus (2) and by dietary folate deficiency (22, 23). Impaired dTMP synthesis leads to genome instability through well-characterized mechanisms associated with uracil misincorporation into nuclear DNA and subsequent futile cycles of DNA repair (24, 25). Nuclear DNA is surveyed for the presence of uracil by a family of uracil glycosylases including: uracil *N*-glycolase (UNG), the single-strand selective monofunctional uracil DNA glycosylase (SMUG), and several others, which scan DNA and initiate base-excision repair (26). Futile cycles of uracil insertion and excision during base-excision repair result in DNA strand breaks and activate a signaling cascade, leading to phosphorylation of serine 139 on histone variant H2AX (γH2AX) in chromatin regions surrounding DNA strand breaks and stalled replication forks, where it forms quantifiable foci (27).

MTHFD1 is a trifunctional enzyme possessing methyleneTHF dehydrogenase (D), methenylTHF cyclohydrolase (C), and formylTHF synthetase (S) activities (15, 18, 28–30). Human mutations in *MTHFD1* cause severe combined immunodeficiency and megaloblastic anemia as a result of disrupted dTMP biosynthesis (18, 31, 32). Human *MTHFD1* polymorphisms are associated with increased risk for NTDs, as well as congenital heart defects (33, 34). Homozygous deletion of *Shmt1* in mouse models is tolerated because of its functional redundancy with SHMT2α, but depresses rates of de novo dTMP synthesis and is accompanied by the development of low-penetrance, folate-responsive NTDs in the form of exencephaly in $Shmt1^{+/-}$ or $Shmt1^{-/-}$ embryos, thus connecting de novo dTMP synthesis to the etiology of folate-responsive NTDs (1, 2, 35). Risk for NTDs is determined by genetic and environmental factors and their interactions (35) and is

Significance

We have identified de novo thymidylate biosynthesis as a target of arsenic at exposure levels observed in human populations. Arsenic enhances methylenetetrahydrofolate dehydrogenase 1 (MTHFD1) small ubiquitin-like modifier (SUMO)-ylation and subsequent proteolytic degradation of MTHFD1 and serine hydroxymethyltransferase (SHMT), resulting in depressed rates of de novo thymidylate synthesis, elevated uracil levels in nuclear DNA, and increased genome instability. These findings provide a molecular mechanism linking clastogenic and teratogenic effects of arsenic to impaired de novo thymidylate synthesis.

Author contributions: E.K., M.S.F., and P.J.S. designed research; E.K., E.R.L., A.C.D., R.P.L., and M.S.F. performed research; E.K., E.R.L., M.S.F., and P.J.S. analyzed data; and E.K., E.R.L., M.S.F., and P.J.S. wrote the paper.

Reviewers: I.D.G., Albert Einstein College of Medicine; and A.P.-M., Dublin City University.

The authors declare no conflict of interest.

[1]To whom correspondence should be addressed. Email: PJS13@cornell.edu.

This article contains supporting information online at www.pnas.org/lookup/suppl/doi:10.1073/pnas.1619745114/-/DCSupplemental.

effectively reduced by folic acid supplementation (36). Arsenic is one of the environmental factors that may contribute to reduced efficacy of folic acid supplementation in NTD prevention (37).

Arsenic is a common environmental toxin, a class I environmental carcinogen (38, 39), and a teratogen in animal models (40). Adverse consequences resulting from chronic arsenic exposure

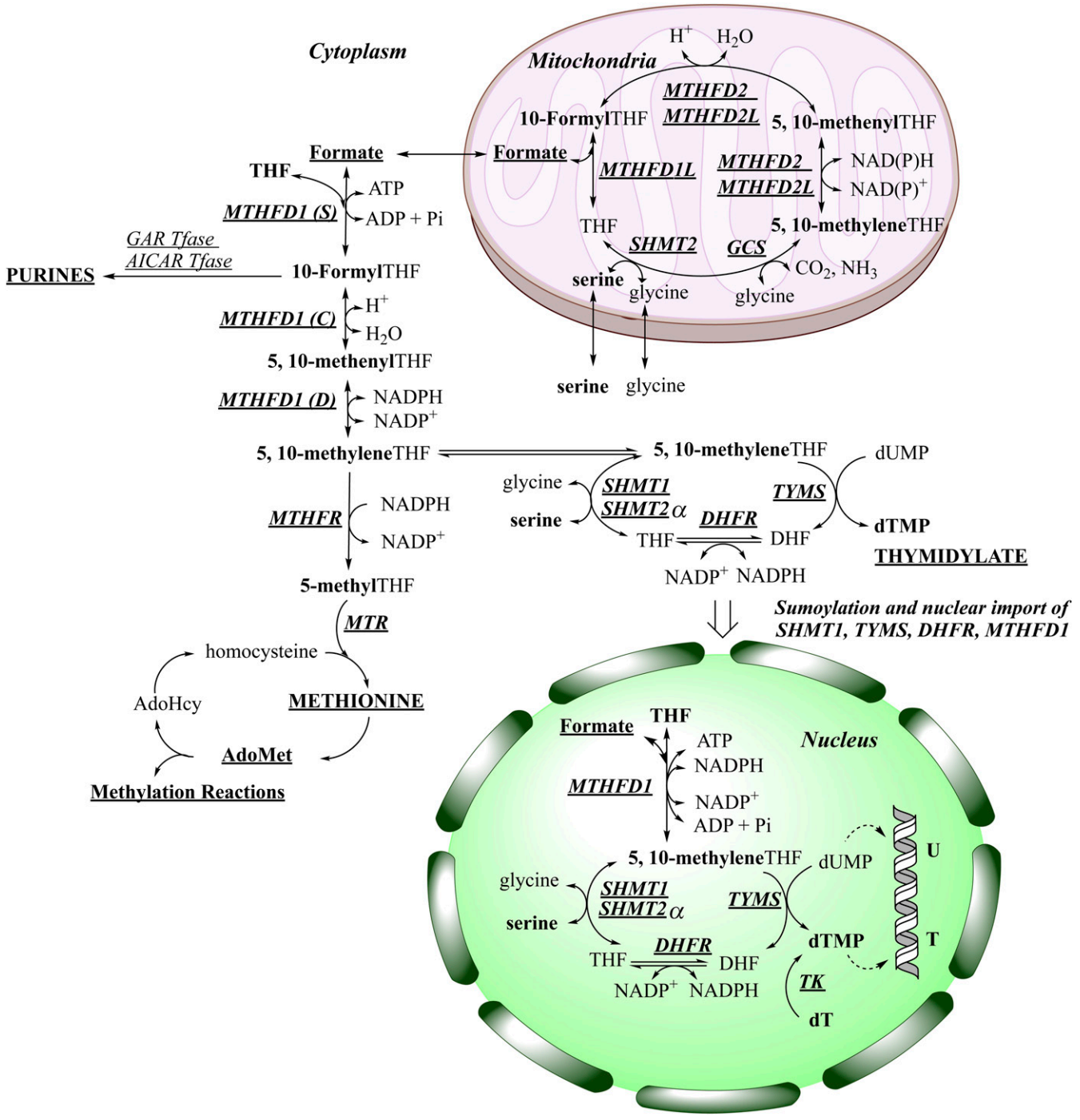

Fig. 1. MTHFD1 and SHMT1 are key enzymes of nuclear de novo dTMP biosynthesis in folate-dependent one-carbon metabolism. Folate-mediated one-carbon metabolism is compartmentalized within the cell. The hydroxymethyl group of serine is a primary source of one-carbon units. Serine enters the pool of activated one-carbon units through the SHMT-catalyzed reaction in the cytosol and mitochondria. In mitochondria, serine and glycine are converted to formate, which traverses to the cytosol and nucleus, where it is condensed with THF by MTHFD1. MTHFD1 is a trifunctional enzyme possessing formylTHF synthetase (S), methenylTHF cyclohydrolase (C), and methyleneTHF dehydrogenase (D) activities. One-carbon metabolism in the cytosol includes the de novo synthesis of purines and the remethylation of homocysteine to methionine. De novo dTMP biosynthesis also occurs in the nucleus, catalyzed by the enzymes SHMT1, SHMT2α, TYMS, and DHFR, which undergo SUMOylation, leading to nuclear import in S-phase. 5,10-methyleneTHF is synthesized by SHMT or MTHFD1 for de novo dTMP synthesis. The *Shmt2* gene is expressed as two transcripts: one that generates SHMT2 for mitochondrial one-carbon metabolism, and SHMT2α, which functions in the cytosol and nucleus. AdoHcy, *S*-adenosylhomocysteine; AdoMet, *S*-adenosylmethionine; AICAR Tfase, aminoimidazolecarboxamide ribonucleotide transformylase; GAR Tfase, glycinamide ribonucleotide tranformylase; MTHFR, methylenetetrahydrofolate reductase; MTR, methionine synthase.

include dermatitis, keratosis, skin cancer, vascular disease, peripheral neuropathy, lung disease and lung cancer, cancers of the kidney and bladder, and neurotoxicity (38, 41). Arsenic trioxide (As_2O_3) is often referred to as a double-edged sword, because it is also a drug approved by the US Food and Drug Administration that is administered in anticancer therapies, alone or in combination with other compounds (42, 43). Importantly, As_2O_3 therapy is efficacious in the treatment of acute promyelocytic leukemia (44), where it is known to affect PML-RARα (promyelocytic leukemia protein and retinoic acid receptor alpha fusion) SUMOylation (45). However, arsenic displays broader cytotoxicity in the absence of the PML-RARα fusion protein, and also at much lower doses than used in As_2O_3 therapy, indicating that other more sensitive biological targets may account for its cytotoxicity and teratogenicity. Here, we demonstrate that arsenic impairs SUMO-dependent nuclear de novo dTMP biosynthesis by targeting MTHFD1, leading to uracil misincorporation into nuclear DNA and increased genome instability, providing a mechanism linking arsenic clastogenicity, toxicity, and teratogenicity to impaired dTMP synthesis.

Results

MTHFD1 Nuclear Translocation During S-Phase Is SUMO Dependent. The enzymes that comprise the de novo dTMP synthesis pathway, SHMT1, TYMS, and DHFR, are SUMO-modified and translocate to the nucleus, where they associate with the DNA replication machinery (13). MTHFD1 has also been shown to localize to the nucleus during S-phase of the cell cycle (14). In this study, the presence of MTHFD1 in nuclei of cells undergoing DNA synthesis was investigated by culturing cells in the presence of 5-ethynyl-2′-deoxyuridine (EdU), a thymidine analog that is incorporated into DNA during synthesis. The MTHFD1-GFP fusion protein was present in nuclei undergoing DNA synthesis, as visualized by EdU incorporation into DNA, whereas MTHFD1-GFP was absent from nuclei that did not incorporate the EdU label (Fig. 2*A*). Human MTHFD1 contains a consensus SUMOylation motif at amino acid residues 222-valine, lysine, glycine, glutamate-225 (222-VKGE-225) (*SI Appendix*, Fig. S1), and has been reported to be a SUMO-modified protein in a proteomics screen (46). In addition, MTHFD1 contains several SUMOylation motifs in a reverse configuration (*SI Appendix*, Fig. S1). Here, we confirmed MTHFD1 SUMOylation in asynchronous HeLa cells by cotransfecting with MTHFD1 tagged with an epitope containing a polyhistidine peptide and a peptide from V proteins of the paramyxovirus of simian virus 5 (MTHFD1-HisV5) and human influenza hemagglutinin (HA)-SUMO-1 constructs (Fig. 2*B*). The identity of the band representing SUMOylated MTHFD1 protein was confirmed by pretreatment with purified ubiquitin-like-specific protease 1 (Ulp1) (a deSUMOylating enzyme, Fig. 2*B*). The identity of SUMOylated MTHFD1 in HeLa cells was also confirmed under denaturing pulldown conditions (Fig. 2*C*) in the presence and absence of purified Ulp1 SUMO protease.

To determine the role of K223 in MTHFD1 SUMOylation and nuclear translocation, an MTHFD1-K223R-GFP mutant protein was generated and characterized in asynchronous and S-phase-arrested HeLa cells. The MTHFD1-K223R-GFP mutant protein exhibited impaired nuclear translocation in S-phase blocked cells compared with the MTHFD1-GFP protein (Fig. 2 *D* and *E*), although nuclear localization of the mutant fusion protein was not completely abolished (Fig. 2*D*). Similarly, the MTHFD1-K223R mutant protein exhibited much less in vitro SUMOylation compared with MTHFD1 protein (Fig. 2*F*). These results support the role of K223 in the SUMO-dependent nuclear trafficking of the MTHFD1 enzyme during S-phase.

As_2O_3 Induces MTHFD1 SUMOylation and Degradation. SUMO-dependent polyubiquitination can lead to increased rates of ubiquitin (Ub)-mediated protein degradation (47), as previously shown for SHMT1 (11). To determine whether MTHFD1 SUMOylation leads to polyubiquitination of the SUMO modification, a MTHFD1-HisV5 construct was coexpressed with GFP alone, a GFP-Ub fusion protein, or a GFP-SUMO-1 fusion protein in HeLa cells (Fig. 3*A*). To assess the SUMOylation and ubiquitination status of MTHFD1, the MTHFD1-HisV5 protein was isolated from HeLa cell lysate, using Ni^{2+} affinity pulldown, followed by Ulp1 SUMO protease treatment (Fig. 3*A*). The GFP protein did not interact with MTHFD1, whereas expression of the GFP-Ub and GFP-SUMO fusion proteins resulted in high-molecular-weight smears above 100 kDa after MTHFD1 isolation, indicating that MTHFD1 is polyubiquitinated and SUMOylated (Fig. 3*A*). When SUMOylated MTHFD1 protein was subjected to Ulp1 treatment, the MTHFD1-associated high-molecular-mass GFP-SUMO1 bands were no longer present (Fig. 3*A*). This indicates that MTHFD1 is covalently modified with SUMO-1 and ubiquitin, and that polyubiquitin-modified MTHFD1 was present, but levels were significantly reduced after Ulp1 treatment (Fig. 3*A*). These results also indicate that MTHFD1 SUMOylation enhanced ubiquitination of the covalently attached SUMO moiety, as illustrated in Fig. 3*B*. In addition to the covalent SUMO modification of MTHFD1 described earlier, MTHFD1 also noncovalently interacted with SUMO (Fig. 3*A*), consistent with the presence of several conserved SUMO-interacting motifs within the MTHFD1 primary sequence (*SI Appendix*, Fig. S2).

Arsenic is known to enhance SUMOylation and degradation of PML-RARα (47), and has been shown to affect TYMS expression levels (48). In vitro SUMOylation of recombinant MTHFD1 protein was enhanced by As_2O_3 pretreatment (Fig. 3*C*). HeLa cells exposed to 5 μM As_2O_3 exhibited increased MTHFD1 SUMOylation (Fig. 3*D*). The protease inhibitor MG132 prevented arsenic-induced depletion of MTHFD1 protein in HeLa exposed to 5 mM arsenic for 3 h, demonstrating that arsenic exposure accelerated rates of MTHFD1 turnover (Fig. 3*E*).

Low-Dose As_2O_3 Exposure Inhibits Thymidylate Biosynthesis. MTHFD1 and SHMT1 turnover was accelerated by 5 μM As_2O_3 exposure (Fig. 4*A*). Low-dose (0.5–2 μM) As_2O_3 treatment also resulted in suppression of de novo dTMP synthesis in a dose-dependent manner (Fig. 4*B*). To determine whether folate depletion could exacerbate the arsenic-induced inhibition of de novo dTMP synthesis, levels of uracil in nuclear DNA were quantified in cells cultured in folate-replete or folate-depleted media treated with and without 1 μM As_2O_3. Depletion of folate from the culture media followed by 1 μM As_2O_3 treatment for 24 h resulted in a pronounced increase in uracil in genomic DNA in Hek293 and in HeLa cells by 283% and 174%, respectively, compared with cells cultured in folate-replete medium without arsenic (Fig. 4 *C* and *D*). This indicates that folate depletion exacerbates the effect of As_2O_3 on uracil DNA content. Low-dose (1 μM for 24 h) As_2O_3 treatment resulted in an increase in genomic uracil levels in HeLa cells and in *Shmt1*$^{-/-}$ mouse embryonic fibroblasts (MEFs) cultured in complete αMEM containing 2.2 μM folic acid and nucleosides by 83% and 140%, respectively, (Fig. 4 *E* and *F*). SHMT1 is an essential scaffold protein for assembly of the nuclear de novo dTMP biosynthesis complex (12). Cells cultured in folate-depleted medium and 1 μM As_2O_3, alone or in combination, resulted in an increase in DNA damage, as measured by phosphorylated histone H2AX (γH2AX) immunostaining in HeLa cells (Fig. 4*G*). Increased levels of γH2AX can result from stalled replication fork movement (49) or as a result of base excision repair pathways that remove uracil from genomic DNA (50) γH2AX immunostaining can be quantified either using percentage of nuclear area covered by γH2AX foci (Fig. 4 *G* and *H*) or using the integrated γH2AX intensity per nucleus (Fig. 4*I*), which is a measure of the brightness of the foci, and by extension, the degree of activation of the genome damage detection pathway. Low-dose As_2O_3 treatment of HeLa cells induced nuclear γH2AX foci and intensity in a dose-dependent manner (Fig. 4 *H* and *I*).

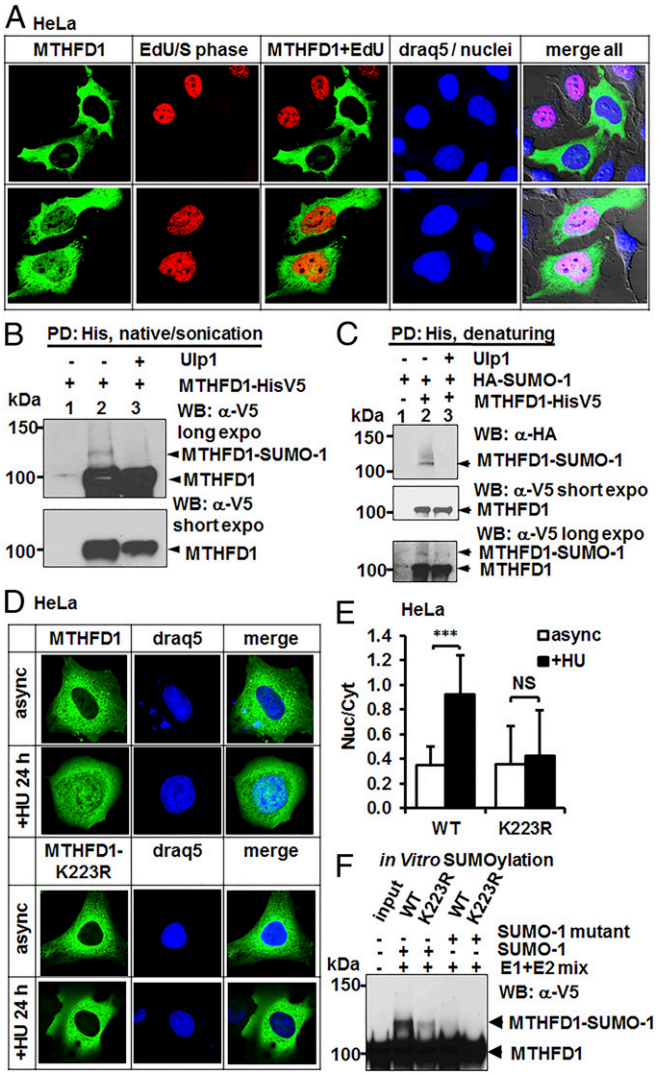

Fig. 2. MTHFD1 translocates to the nucleus in S-phase and is a SUMOylated protein. (*A*) HeLa cells were transfected with MTHFD1-GFP and incubated with a nucleoside analog EdU for 4 h to label cells in S-phase. (*Upper*) MTHFD1-positive cells that did not incorporate the EdU label are also devoid of nuclear MTHFD1. (*Bottom*) MTHFD1-positive cells that incorporated the EdU label (red) simultaneously contain nuclear MTHFD1. (*B*) MTHFD1-HisV5 fusion protein was expressed in HeLa cells (lanes 2 and 3), and MTHFD1-HisV5 protein was Ni^{2+} affinity purified (pulldown, PD) from sonicated total cell lysate. Nontransfected HeLa cells were used as a negative control (lane 1). The MTHFD1 protein migrated at its predicted molecular mass (100 kDa), and an additional higher-molecular mass band was also observed (lane 2, MTHFD1-SUMO). After the pulldown, MTHFD1-HisV5 protein was treated with Ulp1 SUMO protease (lane 3), confirming the identity of the band as SUMOylated MTHFD1 protein. "Long" and "short" refer to relative film exposures. (*C*) HA-SUMO-1 construct, alone (lane 1) or together with MTHFD1-HisV5 construct (lanes 2 and 3), was transfected in HeLa cells, and MTHFD1-HisV5 protein was pulled down from denatured total cell lysate. After the pulldown and washes, isolated MTHFD1-HisV5 protein was treated with Ulp1 SUMO protease (lane 3), confirming the identity of the band as SUMOylated MTHFD1 protein. "Long" and "short" refer to relative film exposures. (*D* and *E*) MTHFD1 is SUMOylated on lysine residue 223. MTHFD1-GFP (WT) or MTHFD1-K223R-GFP fusion proteins were expressed in HeLa cells, and where indicated, cells were arrested in S-phase with 1 mM hydroxyurea for 24 h, fixed, and imaged. Representative images are shown. (*E*) Between 20 and 30 individual cells per condition were scored for nuclear to cytosolic ratio of MTHFD1 fluorescence intensity. Data are presented as mean ± SD, $n > 20$. Statistical significance was determined by Student *t* test. NS $P \geq 0.05$, $^{***}P < 0.001$. (*F*) MTHFD1-HisV5 (WT) or MTHFD1-K223R-HisV5 proteins were expressed in HeLa cells and purified from HeLa lysate soluble fraction by Ni^{2+} affinity purification and used as substrates for in vitro SUMOylation reactions. MTHFD1-HisV5 (WT) (lane 2 and 3) or MTHFD1-K223R-HisV5 proteins were incubated with either SUMO-1 protein or a conjugation-incompetent SUMO-1 mutant protein (lane 4 and 5).

SHMT1 and MTHFD1 Protein Levels Determine Genome Stability. To determine whether the effects of arsenic on genome stability could be attributed to SHMT1 and MTHFD1, the effect of reduced SHMT1 and MTHFD1 expression on genome stability was quantified by measuring levels of DNA-associated γH2AX in HeLa cells treated with validated siRNA constructs (Fig. 5 *A* and *B*) or in MEFs expressing or lacking SHMT1 (*Shmt1*$^{+/+}$ and *Shmt1*$^{-/-}$, respectively; Fig. 5 *D* and *F*). The siSHMT1 and siSHMT2 treatment abolished SHMT1 and SHMT2 expression, whereas the siMTHFD1 treatment resulted in reduced MTHFD1 levels (Fig. 5*C*). The siRNA-mediated decrease in SHMT1 and MTHFD1 proteins was associated with increased genome instability (Fig. 5 *A* and *B*). γH2AX activation, as measured by both quantity of foci and integrated intensity, strongly correlated in all treatments (Fig. 5). These data indicate that arsenic treatment increases γH2AX activation by targeting SHMT1 and/or SHMT2α and MTHFD1.

Shmt1$^{-/-}$ MEFs exhibited increases in both measures of γH2AX activation compared with *Shmt1*$^{+/+}$ MEFs (Fig. 5 *D* and *F*). As_2O_3 treatment further increased genome instability, and the increase was greater in *Shmt1*$^{-/-}$ MEFs compared with *Shmt1*$^{+/+}$ MEFs (Fig. 5 *D* and *F*). Genotype and arsenic each exhibited statistically significant ($P < 0.0001$) effects on percentage nuclear area with γH2AX, and there was a genotype × arsenic interaction ($P = 0.02$). These results demonstrate that the effect of arsenic on genome stability is not limited to cancer cells, and that the effect of arsenic on genome instability can be attributed to its effect on SHMT1 and MTHFD1 levels.

Discussion

Exposure to low doses of arsenic from contaminated drinking water and food can cause cancer, skin lesions (41, 51), cardiovascular disease, diabetes, neurotoxicity, and developmental effects, and can decrease the efficacy of folic acid in NTD prevention (11, 37, 41). Despite mitigation efforts, chronic exposure to low-dose arsenic persists as a global public health issue affecting an estimated 200 million people worldwide (38, 41, 51). Arsenic in contaminated water is present mainly in its most toxic inorganic form, whereas food products contain a mixture of inorganic and less toxic organic forms. The maximum contaminant level of arsenic in drinking water recommended by the World Health Organization and adopted by many countries is 10 μg/L (38, 41, 51). Arsenic in blood is typically 0.3–2 μg/L in people with no known exposure to arsenic, and about 10–15 μg/L and 15–20 μg/L in people exposed to inorganic arsenic in drinking water at 200 μg/L and 400 μg/L, respectively (38). Elevated blood arsenic concentrations (>12 μg/L; equivalent to 0.16 μM inorganic arsenic) and/or total urinary arsenic above 50 μg/g creatinine indicate clinically significant exposure (41). Drinking water or food containing 75 ppb (75 μg/L arsenic) is equivalent in arsenic content to 0.5 μM As_2O_3, the lowest dose assayed in this study (Fig. 4*B*), and would thus expose the rapidly proliferating epithelial cells of the gastrointestinal track to arsenic concentrations shown to affect dTMP biosynthesis in cell culture models in vitro.

Nuclear folate-dependent de novo dTMP biosynthesis limits misincorporation of uracil into DNA and provides a means of cell cycle-dependent regulation of dTMP production (2, 5, 14, 18, 32). Here we show that As_2O_3 concentrations in the range of documented environmental exposures impair folate-dependent de novo dTMP biosynthesis and specifically target SHMT1 and MTHFD1, the two sources of folate-activated one-carbon units in the form of 5,10-methylenetetrahydrofolate. As_2O_3 exposure leads to

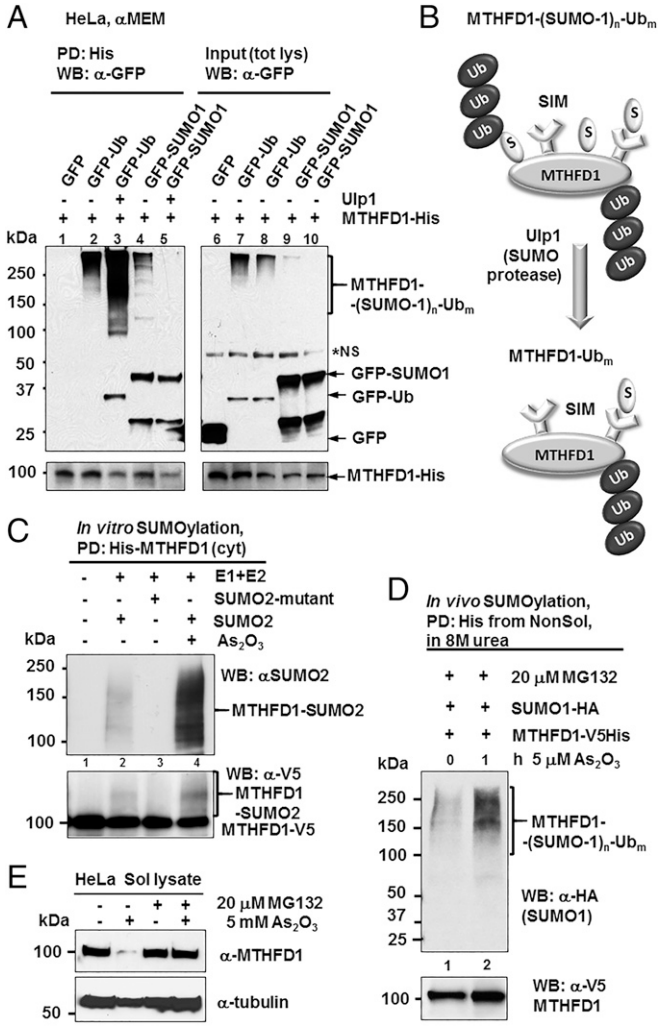

Fig. 3. As_2O_3 targets MTHFD1 for increased SUMOylation and SUMO-dependent polyubiquitination and proteasomal degradation. (*A*) MTHFD1-HisV5 construct was cotransfected with vectors expressing GFP (lane 6), a GFP-Ub fusion protein (lanes 7 and 8), or a GFP-SUMO-1 fusion protein (lanes 9 and 10) in HeLa cells for 48 h. The expression of the transfected GFP fusion proteins and MTHFD1-HisV5 fusion protein was verified in total cellular lysates (tot lys) by α-GFP and α-V5 immunoblotting (input). MTHFD1-HisV5 fusion protein was purified by Ni^{2+} affinity pulldown (PD), followed by Ulp1 SUMO protease treatment (lanes 3 and 5). MTHFD1 SUMOylation and ubiquitination status was assessed by α-GFP immunoblot after MTHFD1 purification by Ni^{2+} pulldown. Nonspecific bands are labeled as NS. (*B*) The proposed model for MTHFD1 SUMOylation and ubiquitination. MTHFD1 ubiquitination is both SUMO-dependent and independent. SUMO interacts with MTHFD1 through both covalent and noncovalent interactions through the SUMO-interacting motif (SIM). (*C*) In vitro SUMOylation of purified MTHFD1 protein in the presence and absence of As_2O_3 (1 mM). (*D*) HeLa cells exposed to 5 μM As_2O_3 exhibited increased MTHFD1 SUMOylation in the presence of proteasomal inhibitor MG132 (E) MTHFD1 protein turnover in the presence or absence of MG132 and/or 5 mM As2O3 for 3 h.

accelerated turnover of SHMT1 and MTHFD1, inhibits de novo dTMP synthesis, increases uracil misincorporation into DNA, and causes genome instability. We also show that low folate culture conditions exacerbate the effects of As_2O_3 exposure on genomic uracil content and genome instability in HeLa cells (Fig. 4), and that *Shmt1* genotype is a modifier of effects of arsenic on genome stability (Fig. 5). Previous studies have shown that SHMT1 undergoes SUMO-dependent ubiquitination in the nucleus, leading to SHMT1 degradation (11). Similarly, these studies demonstrate SUMO-dependent MTHFD1 polyubiquitination and degradation (Fig. 3). Both SHMT1 loss-of-function and arsenic exposure diminish de novo dTMP synthesis capacity, thus providing a mechanism that accounts for their established association with cancer and birth defect risk.

The induction of SUMO-dependent proteolysis of MTHFD1 and SHMT1 by As_2O_3 is reminiscent of the mode of action of As_2O_3 in ATRA-ATO (all-trans retinoic acid and arsenic trioxide) combination therapy and its effect on the PML-RARα fusion protein in acute promyelocytic leukemia. Acute promyelocytic leukemia is a blood disorder that results from chromosomal *t* (15,17)(q22;q12) translocation, creating an oncogenic hybrid protein PML-RARα. RARα is a transcription factor that acts

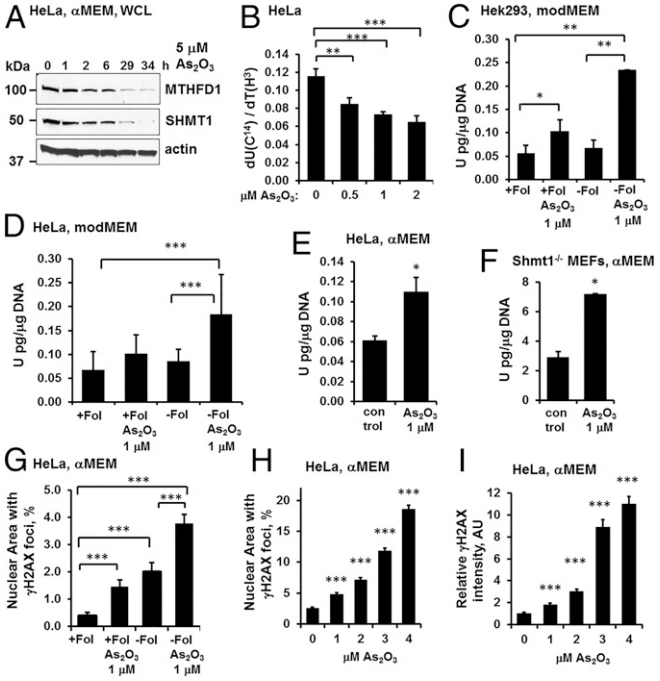

Fig. 4. Low-dose As_2O_3 exposure inhibits de novo thymidylate biosynthesis. (*A*) As_2O_3 induced depletion of SHMT1 and MTHFD1 proteins in a time-dependent manner. HeLa cells were treated with 5 μM As_2O_3 for indicated periods of time before cell lysis. Cell lysates (WCL) were probed with α-MTHFD1 and α-SHMT1 antibodies by immunoblotting. Actin was used to confirm equal sample loading (*SI Appendix*, Fig. S3*A*). (*B*) Low-dose As_2O_3 results in suppression of de novo dTMP synthesis in a dose-dependent manner. The dU suppression assay was used to measure the contribution of the de novo dTMP synthesis pathway (as indicated by [^{14}C]-dU incorporation) relative to the dTMP salvage pathway (as indicated by [^{3}H]-dT). (*C* and *D*) The effect of arsenic and folate on uracil levels in genomic DNA. Cells were cultured in modified MEM (modMEM) with [+Fol, 25 nM (6S) 5-formylTHF] or without [–Fol] (6S) 5-formylTHF in the culture medium and with and without 1 μM As_2O_3 treatment for 24 h in Hek293 (*C*) and HeLa (*D*) cells. (*E* and *F*) The effect of arsenic and folate on uracil levels in genomic DNA in αMEM containing 2.2 μM folic acid. Cells were cultured in αMEM with and without 1 μM As_2O_3 treatment for 24 h in HeLa (*E*) and *Shmt1*$^{-/-}$ MEFs (*F*). One micromole As_2O_3 treatment for 24 h resulted in an increase in genomic uracil in HeLa cells (*E*) and in *Shmt1*$^{-/-}$ MEFs (*F*) cultured in αMEM media containing folic acid and nucleosides. (*G*) The effect of arsenic and folate on nuclear area with γH2AX, a marker of DNA damage. Cells were cultured in modified MEM (modMEM) with [+Fol, 25 nM (6S) 5-formylTHF] or without (–Fol) (6S) 5-formylTHF in the culture medium and with and without 1 μM As_2O_3 treatment for 24 h in HeLa cells. Folate-deficient media and 1 μM As_2O_3 treatment for 24 h increased γH2AX in HeLa cells. (*H* and *I*) As_2O_3 induces nuclear γH2AX foci and intensity in a dose-dependent manner. Data are presented as mean ± SEM. Statistical significance was assessed by Student *t* test in *B*, *C*, *D*, *E*, and *F*, and Mann–Whitney/Wilcoxon test in *G*, *H*, and *I*, with Bonferroni correction. NS $P \geq 0.05$, *$0.01 < P < 0.05$, **$0.001 < P < 0.01$, ***$P < 0.001$.

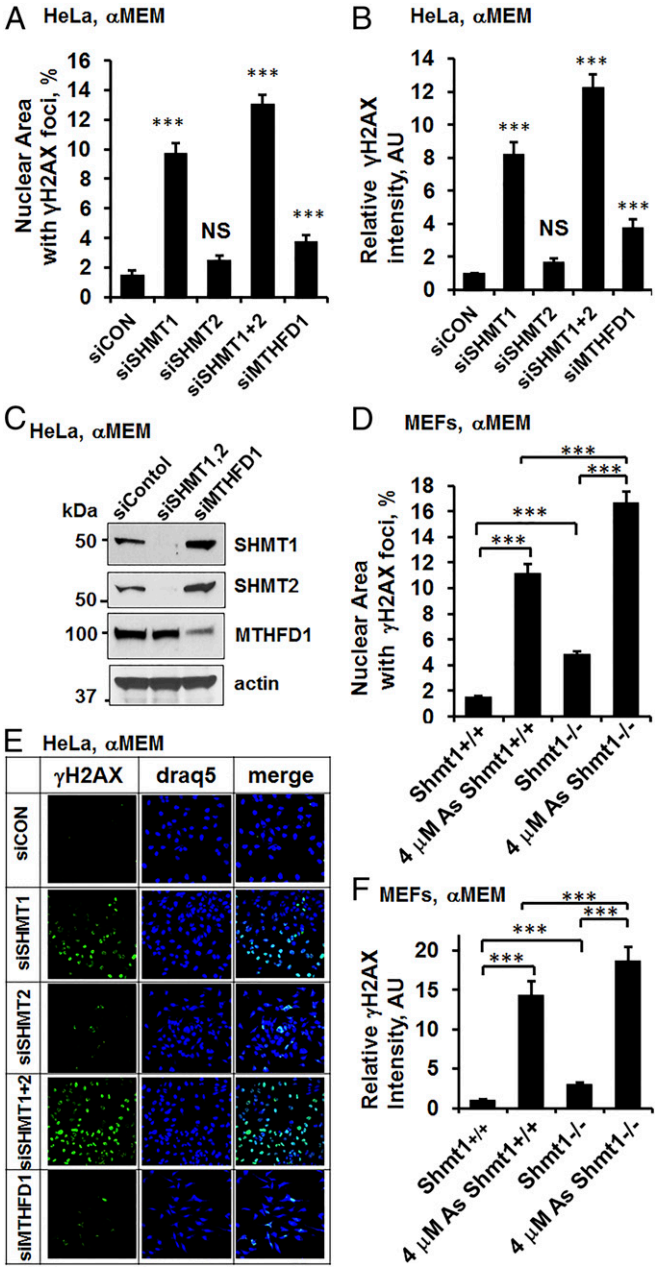

Fig. 5. SHMT1 and MTHFD1 protein expression modulate genome stability. (*A*) Reducing SHMT1, SHMT2, and MTHFD1 expression increases genome instability, shown as percentage nuclear area with γH2AX foci in HeLa cells treated with validated siRNAs. The *P* values (Mann–Whitney/Wilcoxon test) are presented for comparisons with the control condition (siCON) with scrambled siRNAs. (*B*) Reducing SHMT1, SHMT2, and MTHFD1 expression increases genome instability, shown as relative integrated γH2AX fluorescence intensity presented as mean per nucleus ± SEM in HeLa cells treated with siRNA as in *A*. The *P* values (Mann–Whitney/Wilcoxon test) are presented for comparisons with the control condition (siCON) with scrambled siRNAs. Experiments were repeated three times. (*C*) Representative SHMT1, SHMT2, and MTHFD1 immunoblots confirm the efficacy of siRNA treatments in *A* and *B*. Actin was used to confirm equal loading (*SI Appendix*, Fig. S3). (*D*) The effect of SHMT1 expression in MEFs on genome stability. MEFs were cultured for 24 h in αMEM medium containing 4 μM As_2O_3 before fixation. The percentage nuclear area with γH2AX foci was measured as in *A*. (*E*) Representative confocal microscopy images used for γH2AX quantifications in siRNA-treated HeLa cells in *A* and *B*. draq5 (blue, *Middle*) was used as nuclear stain. Ten and 20 images per condition were acquired and analyzed using Metamorph software. (*F*) Relative integrated γH2AX fluorescence intensity presented as mean per nucleus ± SEM in MEF cells treated as in *D*.

together with retinoid X receptors (RXR) to bind DNA and repress transcription in the absence of its ligand retinoic acid. The AML fusion gene encodes a chimeric protein PML/RAR-α with a tighter DNA binding affinity, broader range of binding sites, and stronger repression of transcription, thus blocking myeloid differentiation, which results in the accumulation of malignant promyelocytes in the bone marrow. ATRA therapy induces the terminal differentiation of the leukemic promyelocytes, leading to ATO-triggered apoptosis (45). The PML-RARα fusion protein is endogenously SUMOylated and degraded through its PML moiety, and ATO treatment enhances this proteolytic process, reducing the amounts of repressive RARα (45). The inhibition of de novo dTMP synthesis may contribute to the induction of apoptosis by ATO, as well as more general augmentation of SUMO-dependent polyubiquitation of other cellular proteins. Arsenic exposures at concentrations near environmental exposure levels affect signaling and transcription pathways, including the mitogen-activated protein kinase pathway, p53 localization, the Hedgehog signal transduction pathway, and *c-Myc* expression (52–54). Indeed, the effectiveness of ATO therapy, including in cancers other than acute promyelocytic leukemia, has been studied in more than 140 recent clinical trials registered through ClinicalTrials.gov in colorectal carcinoma, basal cell carcinoma, non-small-cell lung cancer, metastatic kidney cancer, urothelial cancer, advanced neuroblastoma, and others. ATO therapy holds promise when administered in combination with other compounds that target de novo dTMP synthesis, such as 5-fluorouracil, in malignancies such as colorectal carcinoma (55), in combined treatment with itraconazole in refractory metastatic basal cell carcinoma (56), and in combined treatment with gemtuzumab ozogamicin in myelodysplastic syndromes (57). The identification of de novo dTMP synthesis as a target of arsenic suggests other combination therapies including methotrexate, which depletes cellular THF cofactors, and pemetrexed, which in its polyglutamated form is a potent inhibitor of TYMS (58).

In summary, we have identified de novo dTMP biosynthesis as a target of low-dose arsenic exposure by targeting MTHFD1 and SHMT1 stability. The effect of impaired de novo dTMP biosynthesis on genome instability provides a mechanism for the clastogenic and cytotoxic effects of arsenic that may increase risk for arsenic-associated cancers and birth defects that may be prevented by nutritional interventions.

Experimental Procedures

Cell Culture. HeLa and Hek293 cells were maintained in MEM, α-modification (α-MEM; HyClone), supplemented with 10% (vol/vol) FBS. Where indicated (in tracer, γH2AX, and uracil in DNA measurements), the "modified MEM" consisted of α-MEM (HyClone) that lacked glycine, serine, methionine, pyridoxine, folate, and all nucleosides/nucleotides but was supplemented with 10% (vol/vol) dialyzed FBS, 200 μM methionine, 2.5 g/L sodium bicarbonate, 1 mg/L pyridoxine, and 25 nM (6S)5-formyltetrahydrofolate where indicated.

Mouse Embryonic Fibroblast Isolation. For the isolation of $Shmt1^{+/+}$ and $Shmt1^{-/-}$ MEFs, $Shmt1^{+/+}$ and $Shmt1^{-/-}$ females were mated to $Shmt1^{+/+}$ and males to $Shmt1^{-/-}$, respectively. Pregnant dams were killed and embryos harvested at embryonic day 12.5 (E12.5), as described previously (1).

Plasmids. The MTHFD1-GFP construct was generated as previously described (14). The MTHFD1-K223R-GFP construct was generated with the following primers: 5′-CAGCCTGAAATGGTTAGAGGGGAGTGGATCAAAC-3′ and 5′-GTTTG-ATCCACTCCCCTCTAACCATTTCAGGCTG-3′, and MTHFD1-GFP plasmid was used as template with the QuikChange II Site-directed Mutagenesis Kit (Agilent Technologies), according to the manufacturer's protocol. Similarly, the MTHFD1-K223R-V5-His construct was generated using MTHFD1-V5-His as template, using

P values (Mann–Whitney/Wilcoxon test with Bonferroni correction) are graphed as follows: nonsignificant, NS $P \geq 0.05$, *$0.01 < P < 0.05$, **$0.001 < P < 0.01$, ***$P < 0.001$.

the QuikChange II Site-directed Mutagenesis Kit (Agilent Technologies), according to the manufacturer's protocol. The pUlp1 and pGFP-Ub plasmids encoding ubiquitin-like protease 1 and green fluorescent protein-ubiquitin fusion, respectively, were a kind gift of Dr. Volker Vogt, Cornell University, Ithaca, New York. The SUMO-1-HA plasmid was a kind gift of Dr. Olivier Staub, University of Lausanne, Switzerland. GFP-SUMO-1 was subcloned by ligating the SUMO coding region into a linearized pGFP-TOPO vector according to the manufacturer's instructions (Thermo Fisher Scientific). All DNA constructs were sequence verified.

Confocal Microscopy. The plasmids encoding the MTHFD1-GFP or MTHFD1-K223R-GFP fusion proteins (14) were transfected into HeLa cells when 50% confluent, using Fugene 6 (Promega). Cells were plated in duplicates in six-well plates containing 18 × 18 microscopy cover glass #1.5 (Fisher Scientific) on the bottom of each well and were allowed to grow for 36–48 h in α-MEM supplemented with 10% (vol/vol) FBS. Nuclear staining was performed with 5 μM DRAQ5 (Thermo Scientific), according to the manufacturer's protocol. Cell fixation was performed as described (14), with minor modifications. Briefly, cells were washed twice with PBS and fixed with 4% (vol/vol) formaldehyde in PBS for 5 min, washed 4× with PBS, and mounted on microscopy slides with Fluoromount G (SounthernBiotech). Cells were visualized using the Leica SP2 confocal microscope at the Cornell University Microscope and Imaging Facility. Nuclear and cytosolic MTHFD1-GFP signal intensities were quantified using LeicaLite software. The nuc/cyt ratios were calculated for at least 20 individual cells per condition and graphed as mean ± SD. The statistical analysis was performed using bilateral Student's *t* tests for unpaired data. For the EdU labeling of DNA synthesis, cells were incubated for 4 h with EdU, and labeling was performed according to the manufacturer's instructions (Molecular Probes). Where indicated, S-phase cell cycle arrest was performed by incubating cells with 1 mM hydroxyurea (HU) for 24 h before cell fixation. Cell cycle arrest was confirmed by flow cytometry at the Cornell University Microscope and Imaging Facility.

Quantitative γH2AX Methods. Cells were treated as indicated, with indicated concentrations of As_2O_3 for 24 h, or with siRNA (Flexitube, Qiagen, a mix of four preselected, validated siRNAs per gene) with Hiperfect transfection reagent (Qiagen) for 48 h. Cells were fixed in 4% (vol/vol) paraformaldehyde for 10 min, washed 4× with PBS, incubated at 37 °C for 10 min in PBS with 0.5% Triton, then overnight at 4 °C with γH2AX antibody (Millipore) diluted 1:1,000 in PBS with 0.5% Triton, washed 4× with PBS and incubated for 1 h at room temperature in the dark with Dye-light 488 secondary anti-mouse antibody diluted 1:400 in PBS, then washed 4× with PBS.

DRAQ5 DNA stain (Thermo Fisher Scientific) was diluted 1:1,000 (to 5 μM) in PBS and added to the cells for 5 min at room temperature. Coverslips were mounted onto microscopy slides, using 30 μL Fluoromount G (Southern Biotech). All slides for each individual experiment were prepared simultaneously, and all images were acquired in one imaging session with the fixed laser power and gain to allow for quantitation of γH2AX signal intensity. Experiments were repeated 3× with similar results. Images were acquired with the Leica Confocal microscope at the Cornell University Microscope and Imaging Facility. The Metamorph imaging software package (Molecular Devices) was used for γH2AX signal quantifications as follows: γH2AX-positive area was defined as γH2AX signal above a threshold and was expressed as percentage of the total area of the nucleus defined by the DRAQ5 nuclear stain. The percentage of γH2AX-positive area was calculated for each nucleus and presented as a mean ± SEM (n = 420–3,000 cells per condition). Integrated total γH2AX fluorescence intensity per nucleus was also calculated and mean ± SEM graphed. Both measures of γH2AX activation strongly correlated in all experiments. Statistical analysis was performed in JMP software; Wilcoxon/Mann–Whitney test was used for comparisons, and Bonferroni corrections were applied where multiple tests were performed.

In Vitro SUMOylation and DeSUMOylation. HeLa cells were transfected with MTHFD1-V5-His or MTHFD1-K223R-V5-His constructs and lysed 48 h post-transfection at 4 °C in the following lysis buffer: 50 mM Tris·HCl at pH 7.4, 150 mM NaCl, 1% Triton X-100 X-100, and 1:100 diluted protease inhibitor PI mixture (Sigma). The lysates were pelleted at 18,200 × *g* at 4 °C for 10 min and the supernatant was used for the His-tag pulldowns. MTHFD1 proteins were pulled down from the 1% Triton X-100 X-100 soluble fraction (the supernatant fraction containing the pool of non-SUMOylated MTHFD1 protein in HeLa cells), using Dynabeads (Novagen) according to the manufacturer's instructions. Beads were washed 4× with lysis buffer, and the immobilized MTHFD1 protein was used as input for the in vitro SUMOylation reactions (SUMOlink, Active Motif), which were incubated at 30 °C for 3 h with shaking, as directed by the manufacturer. For in vitro de-SUMOylation reactions, Ulp1 SUMO protease was purified and added to the reactions where indicated as 2% (vol/vol), and incubated at room temperature for 15 min.

Protein Immunoprecipitation and Immunoblotting. HeLa cells were transfected with plasmids, as indicated, using Fugene 6 reagent (Promega) for 48 h before cell lysis. For MTHFD1 in vivo SUMOylation experiments, MTHFD1-His protein was pulled down from sonicated total cell lysates supplemented with *N*-ethylmaleimide or, where indicated, from denatured lysate (8 M urea) with Dynabeads (Novagen), according to the manufacturer's instructions. For siRNA experiments, cells were harvested and lysed on ice in a lysis buffer consisting of 150 mM NaCl, 5 mM EDTA, 1% Triton X-100, 10 mM Tris-Cl, and 1:100 dilution of protease inhibitor mixture (Sigma). For the MTHFD1 turnover experiment with proteasomal inhibitor MG132, HeLa cells were preincubated with 20 μM MG132 for 1 h where indicated, and then 5 mM As_2O_3 was added where indicated and cells were incubated for an additional 3 h. As_2O_3 and MG132 were from Sigma. Cells were lysed and lysates spun down, and the soluble lysate fraction was used for immunoblotting. A Lowry-Bensadoun assay was performed to measure protein concentrations. Samples were boiled with Laemmli sample buffer, and 25 μg total protein was loaded to each well of a Tris-glycine SDS/PAGE gel (Thermo Scientific). After separation, gels were washed in transfer buffer for 10 min. Proteins were transferred to a PVDF membrane (Millipore). Membranes were incubated in a blocking buffer containing 5% (wt/vol) BSA in PBS for 1 h and then incubated with primary antibody diluted 1:1,000 for 1 h; α-SHMT1, α-HA, and α-MTHFD1 were from Santa Cruz Biotechnology. Anti-V5 was from Invitrogen. Polyclonal sheep α-SHMT2 antibody was previously described (59), α-SUMO1 and α-SUMO2 antibodies were from Active motif. The in vitro SUMOylation kit and α-GFP were purchased from Sigma. After 3 washes with PBS+0.01% Tween-20, membranes were incubated with HRP-conjugated secondary antibody diluted 1:30,000 in 5% (wt/vol) milk powder in PBS for 1 h. Membranes were developed using chemiluminescent substrate (Thermo Fisher Scientific). Densitometry measurements were performed using ImageJ software.

Quantification of Thymidylate Biosynthesis. HeLa cells were plated in triplicate in six-well plates and allowed to grow for three doublings in modified media supplemented with 200 μM methionine, 1 mg/L pyridoxine, 25 nM (6S)5-formylTHF, 500 nM [^{3}H]-thymidine (Moravek), which is incorporated into DNA by the salvage pathway, and 10 μM [^{14}C]-deoxyuridine (Moravek), which is incorporated into DNA through the folate-dependent de novo dTMP biosynthesis pathway and exposed to a dose of As_2O_3 (0–2 μM). Genomic DNA was isolated using a DNeasy kit (Qiagen) with RNase A treatment, per manufacturer's instructions. Isotope levels were quantified using a Beckman LS6500 scintillation counter in dual disintegrations per minute mode. Experiments were replicated three times.

Uracil Content in Nuclear DNA. Cells were plated and grown for at least four doublings in medium, as indicated (αMEM or modified MEM with or without folate), and were treated with As_2O_3 for 24 h before cell lysis where indicated. Genomic DNA was extracted and uracil quantified as described previously (18), with minor modifications as follows: genomic DNA was purified using Roche DNA extraction kit, then treated with RNase, followed by a second round of DNA purification following the manufacturer's instructions. Uracil was removed from the genome by uracil *N*-glycolase treatment. Uracil was derived and analyzed as previously described (5).

ACKNOWLEDGMENTS. Funding for this study was provided by the National Institutes of Health Grant R37DK58144 (to P.J.S.).

1. Beaudin AE, et al. (2011) Shmt1 and de novo thymidylate biosynthesis underlie folate-responsive neural tube defects in mice. *Am J Clin Nutr* 93(4):789–798.
2. MacFarlane AJ, et al. (2011) Nuclear localization of de novo thymidylate biosynthesis pathway is required to prevent uracil accumulation in DNA. *J Biol Chem* 286(51):44015–44022.
3. Mathews CK (2006) DNA precursor metabolism and genomic stability. *FASEB J* 20(9): 1300–1314.
4. Herbig K, et al. (2002) Cytoplasmic serine hydroxymethyltransferase mediates competition between folate-dependent deoxyribonucleotide and S-adenosylmethionine biosyntheses. *J Biol Chem* 277(41):38381–38389.
5. MacFarlane AJ, et al. (2008) Cytoplasmic serine hydroxymethyltransferase regulates the metabolic partitioning of methylenetetrahydrofolate but is not essential in mice. *J Biol Chem* 283(38):25846–25853.
6. MacFarlane AJ, Perry CA, McEntee MF, Lin DM, Stover PJ (2011) Mthfd1 is a modifier of chemically induced intestinal carcinogenesis. *Carcinogenesis* 32(3):427–433.
7. Hendriks IA, D'Souza RC, Chang JG, Mann M, Vertegaal AC (2015) System-wide identification of wild-type SUMO-2 conjugation sites. *Nat Commun* 6:7289.
8. Hendriks IA, et al. (2014) Uncovering global SUMOylation signaling networks in a site-specific manner. *Nat Struct Mol Biol* 21(10):927–936.

9. Golebiowski F, et al. (2009) System-wide changes to SUMO modifications in response to heat shock. *Sci Signal* 2(72):ra24.
10. Tammsalu T, et al. (2014) Proteome-wide identification of SUMO2 modification sites. *Sci Signal* 7(323):rs2.
11. Anderson DD, Eom JY, Stover PJ (2012) Competition between sumoylation and ubiquitination of serine hydroxymethyltransferase 1 determines its nuclear localization and its accumulation in the nucleus. *J Biol Chem* 287(7):4790–4799.
12. Anderson DD, Woeller CF, Chiang EP, Shane B, Stover PJ (2012) Serine hydroxymethyltransferase anchors de novo thymidylate synthesis pathway to nuclear lamina for DNA synthesis. *J Biol Chem* 287(10):7051–7062.
13. Anderson DD, Woeller CF, Stover PJ (2007) Small ubiquitin-like modifier-1 (SUMO-1) modification of thymidylate synthase and dihydrofolate reductase. *Clin Chem Lab Med* 45(12):1760–1763.
14. Field MS, et al. (2014) Nuclear enrichment of folate cofactors and methylenetetrahydrofolate dehydrogenase 1 (MTHFD1) protect de novo thymidylate biosynthesis during folate deficiency. *J Biol Chem* 289(43):29642–29650.
15. Field MS, Kamynina E, Stover PJ (2016) MTHFD1 regulates nuclear de novo thymidylate biosynthesis and genome stability. *Biochimie* 126:27–30.
16. Woeller CF, Anderson DD, Szebenyi DM, Stover PJ (2007) Evidence for small ubiquitin-like modifier-dependent nuclear import of the thymidylate biosynthesis pathway. *J Biol Chem* 282(24):17623–17631.
17. Tibbetts AS, Appling DR (2010) Compartmentalization of Mammalian folate-mediated one-carbon metabolism. *Annu Rev Nutr* 30:57–81.
18. Field MS, Kamynina E, Watkins D, Rosenblatt DS, Stover PJ (2015) Human mutations in methylenetetrahydrofolate dehydrogenase 1 impair nuclear de novo thymidylate biosynthesis. *Proc Natl Acad Sci USA* 112(2):400–405.
19. Longley DB, Harkin DP, Johnston PG (2003) 5-fluorouracil: Mechanisms of action and clinical strategies. *Nat Rev Cancer* 3(5):330–338.
20. Stover PJ (2011) Polymorphisms in 1-carbon metabolism, epigenetics and folate-related pathologies. *J Nutrigenet Nutrigenomics* 4(5):293–305.
21. Watkins D, Rosenblatt DS (2012) Update and new concepts in vitamin responsive disorders of folate transport and metabolism. *J Inherit Metab Dis* 35(4):665–670.
22. Fox JT, Stover PJ (2008) Folate-mediated one-carbon metabolism. *Vitam Horm* 79: 1–44.
23. Stover PJ (2004) Physiology of folate and vitamin B12 in health and disease. *Nutr Rev* 62(6 Pt 2):S3–12; discussion S13.
24. Blount BC, et al. (1997) Folate deficiency causes uracil misincorporation into human DNA and chromosome breakage: Implications for cancer and neuronal damage. *Proc Natl Acad Sci USA* 94(7):3290–3295.
25. Aherne GW, Brown S (1999) The role of uracil misincorporation in thymineless death. Antifolate *D*rugs in *C*ancer *T*herapy, ed Jackman AL (Humana Press, New York), pp 409–421.
26. Porecha RH, Stivers JT (2008) Uracil DNA glycosylase uses DNA hopping and short-range sliding to trap extrahelical uracils. *Proc Natl Acad Sci USA* 105(31):10791–10796.
27. Rothkamm K, et al. (2015) DNA damage foci: Meaning and significance. *Environ Mol Mutagen* 56(6):491–504.
28. MacFarlane AJ, et al. (2009) Mthfd1 is an essential gene in mice and alters biomarkers of impaired one-carbon metabolism. *J Biol Chem* 284(3):1533–1539.
29. Beaudin AE, Perry CA, Stabler SP, Allen RH, Stover PJ (2012) Maternal Mthfd1 disruption impairs fetal growth but does not cause neural tube defects in mice. *Am J Clin Nutr* 95(4):882–891.
30. Field MS, et al. (2013) Reduced MTHFD1 activity in male mice perturbs folate- and choline-dependent one-carbon metabolism as well as transsulfuration. *J Nutr* 143(1):41–45.
31. Watkins D, et al. (2011) Novel inborn error of folate metabolism: Identification by exome capture and sequencing of mutations in the MTHFD1 gene in a single proband. *J Med Genet* 2011;48(9):590–592.
32. Field MS, Kamynina E, Watkins D, Rosenblatt DS, Stover PJ (2015) New insights into the metabolic and nutritional determinants of severe combined immunodeficiency. *Rare Dis* 3(1):e1112479.
33. Parle-McDermott A, et al. (2006) Confirmation of the R653Q polymorphism of the trifunctional C1-synthase enzyme as a maternal risk for neural tube defects in the Irish population. *Eur J Hum Genet* 14(6):768–772.
34. Christensen KE, et al. (2009) The MTHFD1 p.Arg653Gln variant alters enzyme function and increases risk for congenital heart defects. *Hum Mutat* 30(2):212–220.
35. Beaudin AE, Stover PJ (2009) Insights into metabolic mechanisms underlying folate-responsive neural tube defects: A minireview. *Birth Defects Res A Clin Mol Teratol* 85(4):274–284.
36. Atta CA, et al. (2016) Global birth prevalence of spina bifida by folic acid fortification status: A systematic review and meta-analysis. *Am J Public Health* 106(1):e24–e34.
37. Mazumdar M, et al. (2015) Arsenic is associated with reduced effect of folic acid in myelomeningocele prevention: a case control study in Bangladesh. *Environ Health* 2015;14:34.
38. ATSDR AfTSaDR (2007) Toxicological profile for Arsenic. (US Department of Health and Human Services, Public Health Service, Atlanta). Available at www.atsdr.cdc.gov/toxprofiles/tp.asp?id=22&tid=3. Accessed April 12, 2016.
39. IARC (2004) Arsenic in drinking water. *IARC Monographs on the Evaluation of Carcinogenic Risks to Humans* (International Agency for Research on Cancer (IARC), Lyon, France) Vol 84, pp 39–267.
40. Wlodarczyk BJ, Bennett GD, Calvin JA, Finnell RH (1996) Arsenic-induced neural tube defects in mice: Alterations in cell cycle gene expression. *Reprod Toxicol* 10(6):447–454.
41. IARC (2012) Arsenic and arsenic compounds. *Arsenic, Metals, Fibres, and Dusts*, IARC Monographs on the Evaluation of Carcinogenic Risk to Humans, (IARC, Lyon, France), Vol 100C, pp 41–93. Available at http://monographs.iarc.fr/ENG/Monographs/vol100C/mono100C.pdf. Accessed April 12, 2016.
42. Lai YL, et al. (2003) Combined effect of topical arsenic trioxide and radiation therapy on skin-infiltrating lesions of breast cancer-a pilot study. *Anticancer Drugs* 14(10):825–828.
43. Podolsky L, et al. (2011) 5-Fluorouracil/Leucovorin and arsenic trioxide for patients with refractory/relapsed colorectal carcinoma: A clinical experience. *Acta Oncol* 50(4): 602–605.
44. Platzbecker U, et al. (2017) Improved outcomes with retinoic acid and arsenic trioxide compared with retinoic acid and chemotherapy in non-high-risk acute promyelocytic leukemia: Final results of the randomized Italian-German APL0406 Trial. *J Clin Oncol* 35(6):605–612.
45. de Thé H, Chen Z (2010) Acute promyelocytic leukaemia: Novel insights into the mechanisms of cure. *Nat Rev Cancer* 10(11):775–783.
46. Becker J, et al. (2013) Detecting endogenous SUMO targets in mammalian cells and tissues. *Nat Struct Mol Biol* 20(4):525–531.
47. Lallemand-Breitenbach V, et al. (2008) Arsenic degrades PML or PML-RARalpha through a SUMO-triggered RNF4/ubiquitin-mediated pathway. *Nat Cell Biol* 10(5):547–555.
48. Lam SK, et al. (2014) Downregulation of thymidylate synthase with arsenic trioxide in lung adenocarcinoma. *Int J Oncol* 44(6):2093–2102.
49. Lamm N, et al. (2015) Folate levels modulate oncogene-induced replication stress and tumorigenicity. *EMBO Mol Med* 7(9):1138–1152.
50. Hagen L, et al. (2008) Cell cycle-specific UNG2 phosphorylations regulate protein turnover, activity and association with RPA. *EMBO J* 27(1):51–61.
51. World Health Organization (2008) Guidelines for drinking-water quality: Incorporating first and second addenda (WHO Press, Geneva), 3rd Ed.
52. Huang Y, et al. (2008) Induction of cytoplasmic accumulation of p53: A mechanism for low levels of arsenic exposure to predispose cells for malignant transformation. *Cancer Res* 68(22):9131–9136.
53. Li B, et al. (2016) Arsenic Attenuates GLI Signaling, Increasing or Decreasing its Transcriptional Program in a Context-Dependent Manner. *Mol Pharmacol* 89(2):226–232.
54. Ding W, Tong Y, Zhang X, Pan M, Chen S (2016) Study of arsenic sulfide in solid tumor cells reveals regulation of nuclear factors of activated T-cells by PML and p53. *Sci Rep* 6:19793.
55. Ardalan B, et al. (2010) A phase I study of 5-fluorouracil/leucovorin and arsenic trioxide for patients with refractory/relapsed colorectal carcinoma. *Clin Cancer Res* 16(11):3019–3027.
56. Ally MS, et al. (2016) Effects of combined treatment with arsenic trioxide and itraconazole in patients with refractory metastatic basal cell carcinoma. *JAMA Dermatol* 152(4):452–456.
57. Sekeres MA, et al. (2011) A Phase 2 study of combination therapy with arsenic trioxide and gemtuzumab ozogamicin in patients with myelodysplastic syndromes or secondary acute myeloid leukemia. *Cancer* 117(6):1253–1261.
58. Visentin M, Zhao R, Goldman ID (2012) The antifolates. *Hematol Oncol Clin North Am* 26(3):629–648, ix.
59. Perry C, Yu S, Chen J, Matharu KS, Stover PJ (2007) Effect of vitamin B6 availability on serine hydroxymethyltransferase in MCF-7 cells. *Arch Biochem Biophys* 462(1):21–27.